NJC

ROYAL SOCIETY OF CHEMISTRY

PAPER

View Article Online
View Journal | View Issue

Cite this: *New J. Chem.*, 2023, **47**, 11156

Formation and evolution of channels and voids in gravity sedimentation of kaolin suspensions studied by MRI

Victor V. Rodin * and William M. Holmes

Received 15th March 2023,
Accepted 27th April 2023

DOI: 10.1039/d3nj01214j

rsc.li/njc

Magnetic resonance imaging was employed for the first time to visualize the gravity sedimentation of kaolin suspensions, allowing the internal spatial distribution of kaolin during sedimentation to be investigated. This revealed very complex behaviours dependent on the initial kaolin concentration and solution pH, including vertical channelling, curved channelling, layers/voids and voids only. We show that the number of channels formed increases with the solution pH, with the channels distributed in an evenly spaced-out pattern. The discovery of spontaneous and very stable "void" spaces within the suspension is similar to that previously reported in charged gases (plasmas) and in suspensions of charged Latex particles, which have been explained by the presence of many-body attractive forces. The discovery of such spontaneous voids occurring during kaolin sedimentation, may provide a fundamental explanation for the formation of water channels.

I. Introduction

Gravity sedimentation has great importance in the natural world and in industrial applications, hence it has been studied extensively for several decades.[1–9] Generally, sedimentation of fine particles, with density greater than water, will result in three zones: the supernatant zone, an upper almost clear zone containing very few particles; the suspension zone, where particles/clusters are settling under gravity; and the consolidation zone, *i.e.*, the bottom zone where particles come to rest and compact.[10–12] The sedimentation of non-interacting particles has been well described by theoretical models.[6,7,13–16] However, the sedimentation of charged interacting particles remains largely unsolved.[17–21]

DLVO theory has been widely used in colloidal chemistry to explain the stability of dilute colloidal dispersions.[17–19,21–23] If electrostatic repulsion between particles is large, the suspension is stable; if repulsion is weak, flocculation can occur. In sedimentation experiments, flocculation increases particle size increasing the rate of settling.[4,6,10,14] However, DLVO theory cannot explain some experiments of highly charged colloidal suspensions which demonstrate vapour–liquid coexistence, biphasic regions, and void structures.[17,19,23] Large and stable void structures have been found in polymer latex dispersions, with dimension of up to 150 μm.[23–25] Such voids have also been demonstrated in dusty plasmas, with centimetre sized regions completely free of dust.[26]

A common, but not widely recognised, phenomena known as channelling[1,4,10,11] is defined as the creation of vertical flow paths on a scale much larger than the size of the solid particles themselves.[27] This phenomenon has been observed visually *via* the formation of "volcanoes" at the interface of the supernatant and suspension zone at the end of sedimentation.[1,10,14] The channels are thought to act as vertical paths for fluid flow, allowing water to escape the settling suspension at a high rate, thus increasing the interface settling velocity.[11] Channels paths have previously been seen using glass wall cells, or in compacted mud when cut open.[8,10–12] Some studies have also shown that particles moving up through the channels towards surface, leading to the development of volcanoes at interface of the supernatant and suspension zones.[1,4,8,10,11,14] Settling characteristics and consolidation microstructure of sediments can be strongly affected by channels and such factors as confined flows, interparticle forces, or activated transitions in colloidal suspensions/dispersions.[28–31] Some approaches based on interaction of kaolinite materials with water have been developed[32,33] to model settling velocity in sediments and microstructure of kaolinite suspensions. The phenomena of channelling has been studied for such materials as calcite, aragonite, talc, attapulgite, activated sludge, calcined kaolin, hydrous kaolin.[1,8,10,11] Kaolin is a mixture of the mineral kaolinite (rich in kaolinite) and other minerals, *e.g.*, quartz, anatase, feldspar, muscovite. Kaolinite is a clay mineral with the chemical composition $Al_2Si_2O_5(OH)_4$. It is a layered silicate mineral, with tetrahedral sheets of silica (SiO_4)

Glasgow Experimental MRI Centre, Institute of Neuroscience and Psychology, College of Medical, Veterinary and Life Sciences, University of Glasgow, Glasgow, G61 1QH, UK. E-mail: victor.rodin@jku.at

linked through oxygen atoms to octahedral sheets of alumina (AlO_6). Kaolin platelets have a negative charge on the basal surface, due to substitution, and a positive change on the surface edges due to broken bonds.

Magnetic Resonance Imaging (MRI) has the ability to non-invasively image nuclei with a non-zero magnetic moment, such as ^1H in water molecules. Thus, MRI is allowing three dimensional imaging of opaque media and yielding their internal structure. Though often associated with clinical diagnosis, MRI has been widely used to investigation phenomena in the physical and engineering sciences, such as oil recovery, reactors, rheology, and riverbed dynamics.[34] Indeed, MRI has previously been used to study various sedimentation processes.[35–38]

Here we use MRI to non-invasively image the sedimentation of kaolin *in situ*, allowing the formation and evolution of voids/channels to be monitored. Further, the effects of kaolin concentration and pH on the rate of settling and microstructure were investigated.

II. Materials and methods

A. Preparation of samples

The anhydrous kaolin ($Al_4Si_4O_{10}(OH)_8$) used in this study was supplied by Merck Ltd (SIGMA-Aldrich). Solutions with various values of pH were prepared using alkaline/acid additives (KOH, HCl) and buffers and checked with a Benchtop pH meter using standard laboratory calibration solutions with buffers. The suspensions were placed in glass bottles of cylindrical shape (height = 48 mm, diameter = 25 mm) with caps. Eight different kaolin concentrations have been tested, ranging from 22.9 to 90.7 g L^{-1}, at six values of pH: from pH 1.9 to pH 13.0. To ensure proper mixing, the samples were placed in a vibration mixer (with frequency of 6 Hz) for 5 min. After vibration, the samples were quickly fixed inside the RF coil and placed inside the bore of the MRI scanner.

B. MRI setup and measurements

MRI experiments with kaolin suspensions were carried out on a horizontal Bruker PharmaScan Avance III imaging system operating at 300 MHz for protons (Bruker, BioSpin, Germany). T_2-weighted imaging was performed using a rapid acquisition with relaxation enhancement (RARE) pulse sequence. To image the whole cylindrical sample volume, 17 horizontal cross-section slices were acquired, each with a slice thickness of 2 mm, with the top slice imaging the top of the supernatant, and the bottom slice imaging the bottom of the sample. Examples of cross-sectional images are shown in Fig. 2 and 9. MRI cross-section scanning was performed with following

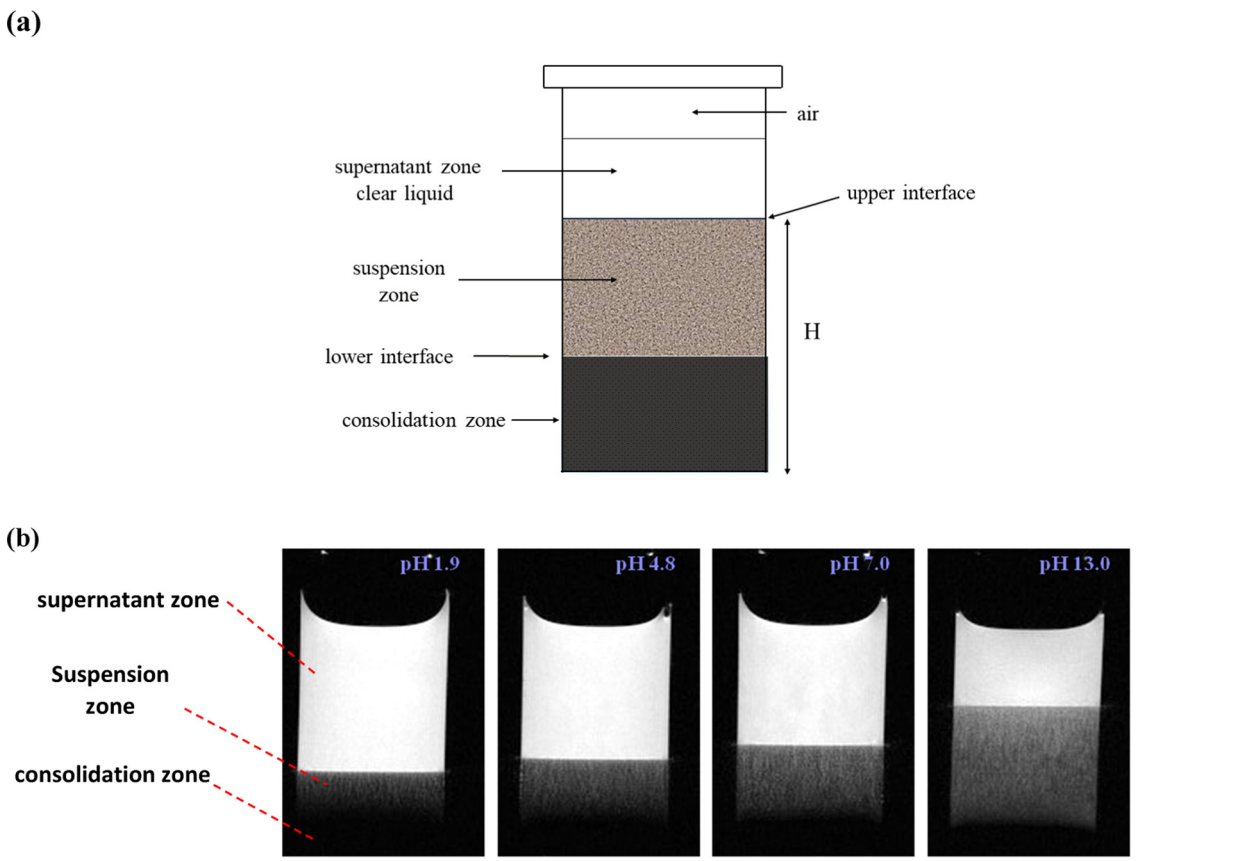

Fig. 1 (a): Schematic diagram of kaolin suspension showing supernatant, suspension, and consolidation zones. (b) Example images demonstrating the effect of pH on the rate sedimentation, images acquired between 11–13 min after the start of sedimentation (22.9 g L^{-1} kaolin). The supernatant zone is nearly pure water and shows white, the sedimentation zone shows grey and the consolidation zone shows black.

experimental parameters: field of view (FOV) = 2.70 × 3.20 cm; repetition time (TR) = 5000 ms; echo time (TE) = 34.1 ms; Matrix 108 × 128; number of averages (NA) = 4; RARE factor = 12; scan acquisition time (TA) = 2 min 20 s. Acquisition of the 17 horizontal slices are performed simultaneously, not slice by slice. The in-plane spatial resolution of the cross-sectional MRI images was 0.25 mm × 0.25 mm. It should be noted that the MRI signal is averaged over the 2 mm thickness of the MRI slice.

To visualised vertical sections of the kaolin samples, 4 vertical slices were imaged. These 1 mm thick slices were centred covering the middle of the circular cross-section, see Fig. 3. MRI vertical scanning was performed with the following experimental parameters: FOV = 5.0 × 3.20 cm; TR = 5000 ms; TE = 17 ms; ST = 1 mm; Matrix 200 × 128; NA = 1; RARE factor = 4; TA = 2 min 40 s; NS = 4. The in-plane spatial resolution of the vertical MRI images was 0.25 mm × 0.25 mm. Examples of vertical section images are shown in Fig. 1, 2(top), 3, 7 and 10.

The temporal evolution of the sedimentation process was monitored by alternately acquiring the horizontal images (scan time 2 min 20 s) and then the vertical images (scan time 2 min 40 s). This alternation was continually repeated over a 4 h period.

The MRI signal comes solely from the hydrogen nuclei present within water molecules. However, this signal is weighted by the loss of signal due to T_2-relaxation, where the rate of relaxation R_2 ($R_2 = 1/T_2$) increases with increasing concentration of kaolin. The MRI signal, S, from a particular voxel is given by,

$$S = S_0 f \mathrm{e}^{\left(\frac{-t}{T_{2,\mathrm{f}}}\right)} \quad (1)$$

where S_0 is the signal from a 100% water filled voxel, f is the fraction of water within the voxel and $T_{2,\mathrm{f}}$ is the relaxation time of water for a water fraction of f. On T_2-weighted MRI images, water shows bright white (high signal) and the kaolin suspension as grey (moderate signal). At high kaolin concentrations, the T_2 relaxation is sufficient to completely kill the MRI signal. This can be seen in Fig. 1, 3 and 7, where there is no signal from the consolidation zone.

C. Image and data analysis

Fig. 1(a) presents a schematic diagram of a kaolin suspension showing supernatant, zone of sedimentation and consolidation zone. To quantify the sedimentation of kaolin particles, the height H was measured from the bottom of sample to the position of interface between supernatant and suspension zone (upper interface) using the vertically sliced MR images. For example, Fig. 1(b) presents several images of vertical slicing at settling kaolin suspensions (22.9 g L^{-1}), showing how the rate of kaolin sedimentation decreases with increasing pH.

To measure the number of channels seen in the cross-sectional MRI images (Fig. 2) and in vertical MRI slicing (Fig. 1(b) and 3), the MRI slices were combined to form a 2D-data matrix. The signal intensities of the voxels were then normalised using the average signal of the voxels in the supernatant. The average signal of the supernatant was considered as representing the signal from a 100% water filled voxel. The normalised data matrix was then threshold (90%) to identify clusters of voxels forming channels. It should be noted that the number of channels identified by this approach was slightly sensitive to the threshold applied (*e.g.* 85%, 87%, 90% were tried). However, this did not change the trend, whereby the number of channels increased with pH.

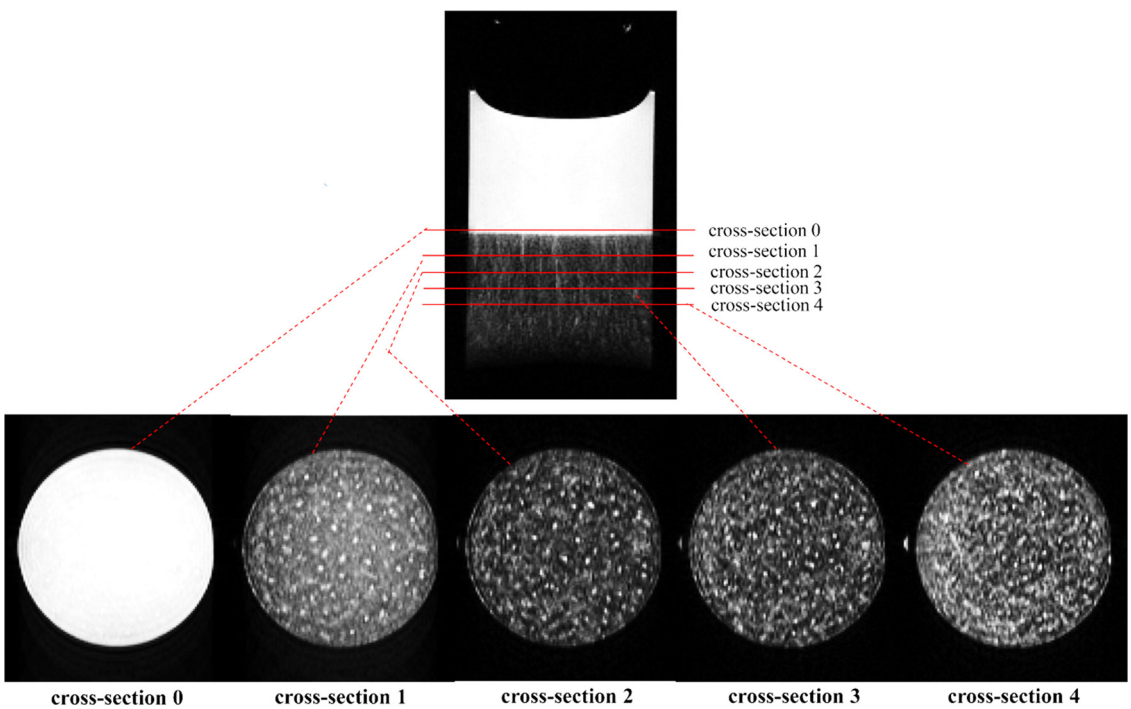

Fig. 2 Example cross-sectional slices showing the channels formed in the suspension zone (25.0 g L^{-1} kaolin, pH 8.8, sedimentation time 10 min.

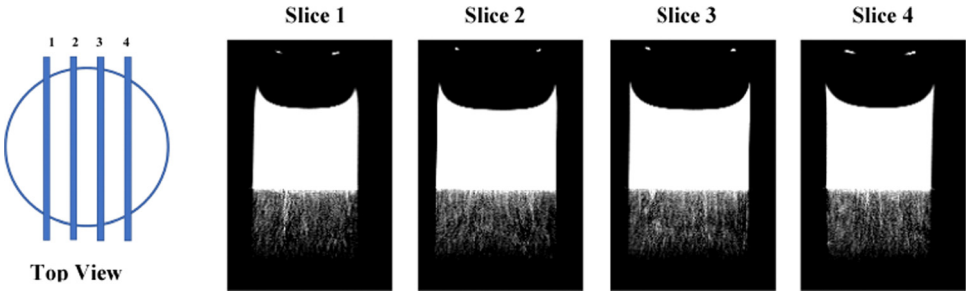

Fig. 3 Schematic diagram, showing the position of the four vertical slices. Example vertical images demonstrate the formation for vertical channels (25.0 g L^{-1} kaolin, pH 1.9, sedimentation time 13 min). The central slices 2 and 3 were used for analysis. The supernatant zone is nearly pure water and shows bright white, the sedimentation zone shows grey, and the consolidation zone shows black. Vertical channels within the suspension zone show white.

III. Results

A. Rate of sedimentation: effect of pH and kaolin concentration

A series of sedimentation experiments were performed using different initial kaolin concentrations and different solution pH, with the rate of sedimentation clearly dependent on both parameters. Fig. 1 shows how the rate of kaolin sedimentation slows with increasing pH. Also, this study showed that the lower interface, between the suspension zone and the consolidation zone, is much less district than the upper interface between the supernatant and suspension zone. Fig. 4 shows how the height, H, of the upper interface of the suspension zone, varies with time and pH.

The results shown in the Fig. 5 demonstrate how H varies with pH, for a varying concentration and a fixed sedimentation time. At lower kaolin concentrations, sedimentation becomes slower at increasing pH. Whereas, as kaolin concentration increases, the effect of pH decreases, until at the highest concentrations (*e.g.*, 60.7 and 90.7 g L^{-1}) pH has little effect on the rate of sedimentation. The same dataset is plotted in a different fashion in Fig. 6, demonstrating how H varies with kaolin concentration, for a fixed sedimentation time. For instance, for low kaolin concentrations (22–32 g L^{-1}), Fig. 6(a) shows that the curves of H-dependences on kaolin concentration are different for various acidities in the range of pH 1.9–8.8. The larger the pH value, the steeper the slope of the curve. Note, attempts were made to image kaolin concentrations below 22.9 g L^{-1}, however, the sedimentation process was too fast. This meant that the kaolin suspension had already settled before the sample could be transferred to the MRI and scanned.

B. Channelling and voids in the kaolin suspensions

The kaolin did not always settle uniformly, under certain conditions channels, layer and voids were seen to form. Fig. 7 presents a phase diagram showing which structures (channels, layers, or voids) were formed at different initial kaolin concentration and pH. On the T_2-weighted MRI images of vertical slices, water shows bright white (high signal), the kaolin suspension as grey (moderate signal) and the consolidated kaolin shows black (low signal). On the cross-sectional T_2-weighted images (Fig. 2), the water channels and voids show up clearly as hyperintense, *i.e.*, high water and low kaolin content. Fig. 3 shows the channels occurring in all 4 vertical slices for one example of kaolin suspension with solids 25.0 g L^{-1} at pH 1.9.

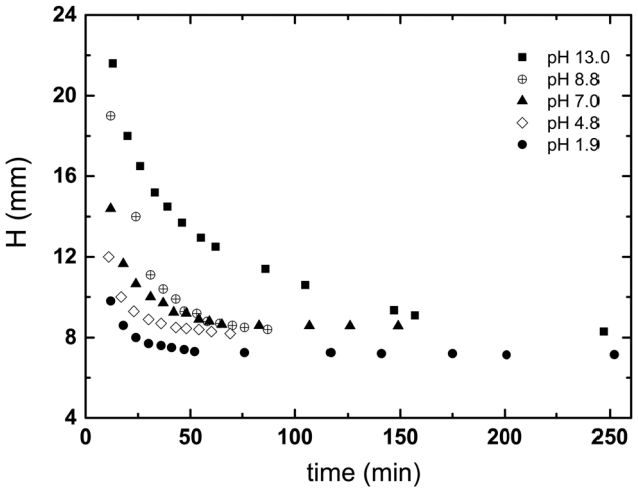

Fig. 4 Dependences of interface H (mm) in images of kaolin suspensions with solid concentration of 22.9 g L^{-1} in the samples with different pH (from pH 1.9 to pH 13.0) on the sedimentation time.

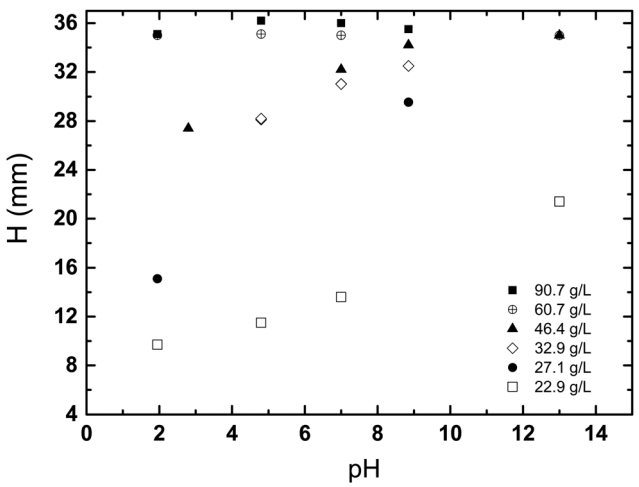

Fig. 5 The dependences of interface H in the images of kaolin suspensions for first measurable scans (11–13 min after placement of sample in the magnet) on pH at various solids from 22.9 g L^{-1} to 90.7 g L^{-1}.

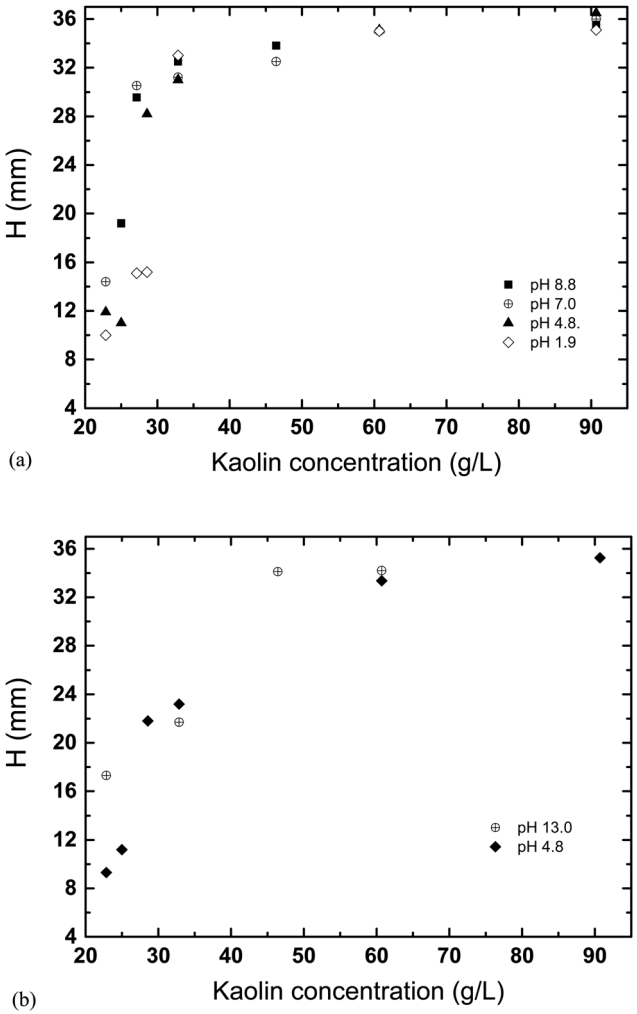

Fig. 6 The interface H in images of kaolin suspensions at sedimentation time of 11–13 min (a) and 23 min (b) as a function of kaolin concentration at various pH: (a) pH 8.8; 7.0; 4.8; 1.9; (b) pH 13.0 and pH 4.8. Initial value of H (before MRI scanning) was 36 mm for all samples.

Channelling. For low initial kaolin concentrations ($\sim$23 g L^{-1}) vertical channels formed at the top of the suspension zone, starting at the interface and moving down. Examples of such vertical channels are shown in the T_2-weighted MR images presented in Fig. 1(b) and 3. The length of the channels ranged from approximately 0.5 mm to 7 mm. The diameter of the channels cannot accurately be measured from the MR images, as it was close to the in-plane resolution of the MR images (300 μm). However, we estimate the diameter varied from $\sim$0.3 mm to 2 mm.

Analysing the cross-section images of the 22.9 g L^{-1} kaolin suspension, we found that the number of vertical channels, N, increased with increasing pH (Fig. 8). At higher kaolin concentrations (27.1–46.4 g L^{-1}), the channels become less vertical and more curved/tortuous. Examples of this are shown in Fig. 7.

Complex layers and voids. At intermediate kaolin concentrations (46–61 g L^{-1}), individual channels could not be identified, instead complex layers/patterns of different kaolin concentrations formed in the suspension zone. Cross-section images presented in the Fig. 9 for kaolin suspensions with solids amount 46.4 g L^{-1}

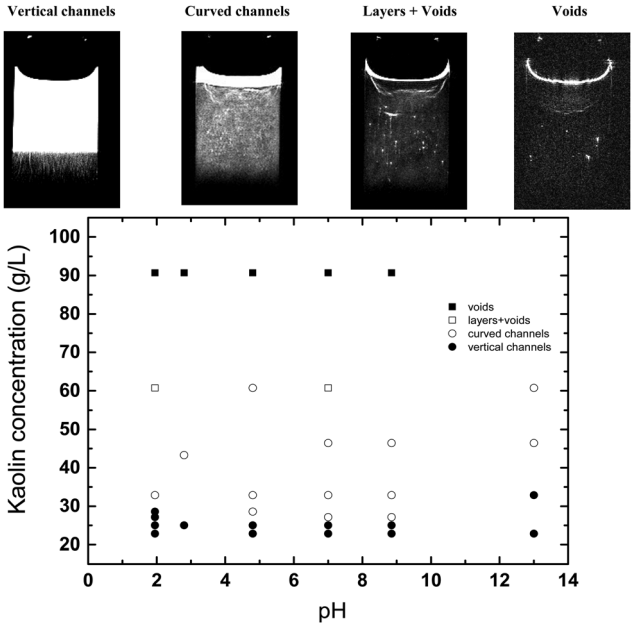

Fig. 7 Phase diagram showing the relationship between the initial solid concentration, pH value and the four types of behaviour that were observed (*i.e.* vertical channels, curved channels, layers/voids and voids) Top: Example images exhibiting the four different types of behaviour seen during kaolin sedimentation.

for various pH (pH 7.0, pH 8.8 and pH 13.0), show complex pattern with layers and voids without ordered structures. Though, voids of water can be seen in some cross-sectional images, these did not show as channels that ran through multiple cross-sections. Hence, a quantitative comparison of the number of channels N in these images was not possible.

Voids. Finally, at high kaolin concentration ($\sim$90 g L^{-1}), approximately spherical regions of water, voids of kaolin (termed

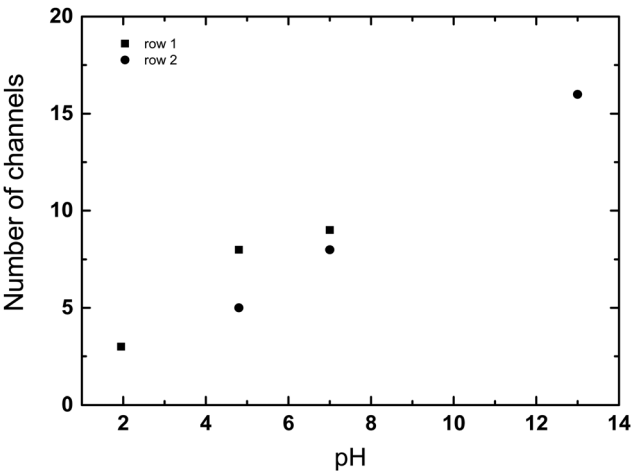

Fig. 8 The number of vertical channels, N, was calculated from the matrix data using a 90% threshold, for an initial kaolin concentration of 22.9 g L^{-1} (sedimentation time 11–13 min). Plot is shown for the data of first row (black squares, pH 1.9–7.0) and second row (black circles, pH 4.8–13.0) of matrices data describing the images, *i.e.*, those rows of cell array which are nearest to interface between supernatant and suspension zone.

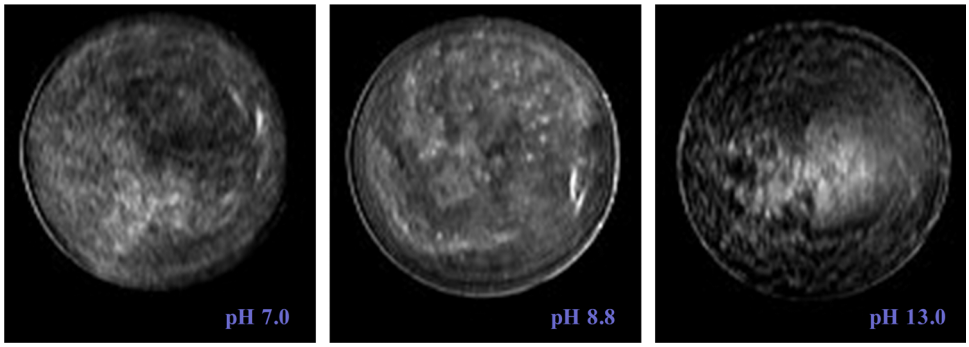

Fig. 9 The images of kaolin suspensions at solid concentrations 46.4 g L^{-1} with different pH: pH 7.0, pH 8.8, and pH 13.0.

"voids"), formed in the suspension zone, see Fig. 10. These voids were found to be stable over the whole MRI scanning time (~24 h).

Fig. 10 shows the images of vertical slices for the suspensions with largest initial kaolin amount (90.7 g L^{-1}) in studied samples. At these kaolin concentrations, there was no clear interface separating the suspension and consolidation zones. In the MRI images most of the sample below the supernatant was black, *i.e.* no signal. This does not mean there is no water present, just that this water has experienced rapid T_2 relaxation due to the high concentration of kaolin. However, several bright spots with intensities comparable with that found in supernatant were observable. These bright spots have very low kaolin concentration (*i.e.* void of kaolin), and were stable over several hours, hence we have termed them "stable voids". These stable voids were discovered for all studied pH values for the highest initial kaolin concentration studied (90.7 g L^{-1}).

IV. Discussion

$$H_2SiO_3 \Leftrightarrow SiO_3^{2-} + 2H^+ \quad (2)$$

Kaolin is rich in kaolinite ($Al_2O_3{\cdot}2SiO_2{\cdot}2H_2O$), when in contact with water the surface of SiO_2 groups interacts with water, resulting in a particle with a negatively charged surface, compensated by ions of opposite charge present in the liquid phase (electric double layer). There have been numerous previous studies investigating the sedimentation of kaolin suspensions.[1,10,11,32,33] For example, the work of Nam *et al.*[10] employed kaolin concentrations in the range of 1.01 to 1.2 g cm^{-3} (with KCl). At these high kaolin concentrations, the rate of sedimentation is very slow and independent of pH. Here particles are close together and electrostatic interactions are strongly repulsive, which slows sedimentation and overwhelms the effect of solution pH. Furthermore, during gravity sedimentation of kaolin, the formation of water channels has been previously observed.[10,11] Initially, the presence of water channels was indicated by the formation of "volcanos" on the surface of the suspension zone,[11] where the volcanos are formed from kaolin particles transported upward by flow of water in the channels. However, in later experiments, the channels have been visually observed by employing glass windows.[10] It has been argued that this channelling effect is linked to the flocculation of kaolin particles at these high concentrations, whereby the water channels provided a path to reduce excess pore pressure and a means for the exit of water upwards.[11,12]

For the first time, this study uses MRI to non-invasively image the sedimentation process both dynamically and *in situ*. However, it should be stressed that the range of initial kaolin concentrations employed here (22.9 to 90.7 g L^{-1}), are

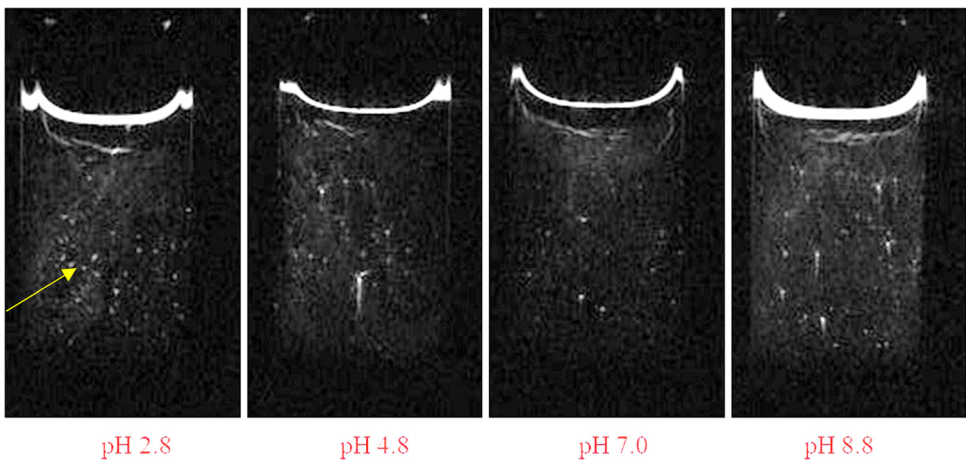

Fig. 10 Images of kaolin suspensions with initial solids of 90.7 g L^{-1} for various pH values: pH 2.8, 4.8, 7.0, and pH 8.8. At this high kaolin concentration stable kaolin voids (bright white spots) were observable which did not change during several hours of MRI scanning. Yellow arrow points to examples of stable voids.

an order of magnitude lower than in other published literature.[1,10,11,32,33] In agreement with previous studies,[10] we found no flocculation of kaolin particles at these low kaolin concentrations. Further, we found the rate of sedimentation increases as the initial kaolin concentration is decreased (Fig. 6), and that the rate of sedimentation is dependent on pH (Fig. 4). Again, these observations can be explained by electrostatic interactions, where at lower concentrations the kaolin particles are further apart and experience less repulsive forces, resulting in faster sedimentation. In addition, these lower repulsive forces are now affected by solution pH, with the rate of sedimentation increasing with lower pH (Fig. 4). For instance, the typical average velocity of the moving interface at the time of the first MRI, have been estimated as 1.11 mm min^{-1} (pH 13), 1.41 mm min^{-1} (pH 8.8) and 2.18 mm min^{-1} (pH 4.8). It should be noted that very high pH can potentially alter the micromorphology and micromechanics of the kaolin particles, which may also affect their sedimentation.[33]

MRI is not essential to measure the rate of sedimentation, as the height H of the supernatant interface can very easily be visualised and measured with a ruler. Where MRI is special, is its ability to non-invasively observed the internal spatial distribution of kaolin during sedimentation. This has revealed some very complex behaviour, that we have categorised as either vertical channelling, curved channelling, layer/voids and voids only. As can be seen in Fig. 7, the type of behaviour was strongly determined by initial kaolin concentration and was largely independent of solution pH.

At the lowest initial kaolin concentration (22.9 g L^{-1}), we found that vertical water channels spontaneously formed, reaching down from the supernatant interface into the suspension zone. This can be very clearly seen in Fig. 2, where the cross-sectional images show ~60 vertical channels have formed, which are approximately evenly spaced. The channels are of varying lengths and we estimate their diameters range from approximately 0.3 mm to 2 mm. At higher kaolin concentrations (27.1–46.4 g L^{-1}), the channels become less vertical and more curved/tortuous, examples of this are shown in Fig. 7. At intermediate kaolin concentrations (46–61 g L^{-1}), individual channels could not be identified, instead complex layers/patterns of different kaolin concentrations formed in the suspension zone, see Fig. 9. At the highest kaolin concentration (90.7 g L^{-1}) approximately spherical regions of water (~1 mm diameter), void of kaolin, were observed. These kaolin voids were remarkably stable over several hours. It is important to note that even at our highest kaolin concentration (90.7 g L^{-1}), we observed no evidence of flocculation, which occurs at higher kaolin concentrations.

When considering the MR images, it is worth remembering that they are weighted by T_2 relaxation, the effect of which increases with increasing kaolin concentration. This can be seen in Fig. 1, 3 and 7, where there is no signal from the consolidation zone. This fact is worth bearing in mind when considering channelling. Once the kaolin has consolidated, there may still be water channels fixed within the consolidated structure, but these channels may not be visible on MRI.

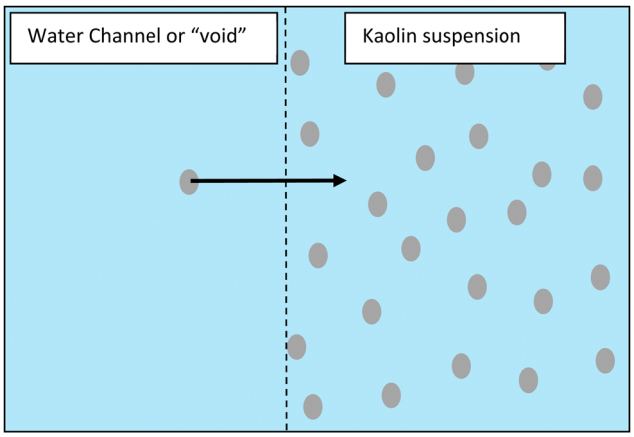

Fig. 11 Even though kaolin particles are negatively charged and repel, it has been argued that a particle at the interface must experiences a net attractive force preventing particles from diffusing into the channel/void space (*i.e.*, many body attraction).[25]

Indeed, in the literature such fixed channel structures have been observed in consolidated sediment.[1,8,10]

Our discovery of approximately spherical regions of water, void of kaolin (Fig. 10), that form in the suspension zone are extremely interesting and may help to identify a mechanism for the formation of water channels. These voids were very stable and in some cases did not change over several hours. These results are very similar to previous studies, which found void spaces spontaneously occurring in plasma (ionised gas)[26] and in highly purified polymer latex dispersions.[23–25] How these voids are able to form and be stable over long periods of time is fascinating. It has been argued that the reason a particle at the void/suspension interface is prevented from diffusing into the void is the presence of net attractive forces (*i.e.*, many body attraction), see Fig. 11. Warren has proposed a development of Debye–Huckel theory for highly asymmetric electrolytes as a theoretical explanation.[25]

We hypothesise that the spontaneous formation of stable voids at our highest initial kaolin concentrations (90.7 g L^{-1}), provides a mechanism for the formation of water channels seen at lower initial concentrations. At high kaolin concentrations the voids were stationary, presumably the buoyancy force on the void not being sufficient to overcome repulsive force within the kaolin suspension. However, we speculate that at lower kaolin concentration, the buoyancy force of the void, leads to elongation of the void, eventually creating a vertical water channel. The effect of pH on channel formation is also intriguing, with the number of channels formed increasing with increasing pH (Fig. 8). This indicates that increased repulsive forces between particles are favourable to channel formation. Further, it is interesting to note that the channels do not form at random locations, but rather show the appearance of being evenly spaced out.

V. Conclusion

Magnetic resonance imaging was employed for the first time to visualize the sedimentation of kaolin suspensions. This

approach showed that channelling phenomena occur at much lower kaolin concentration than previously thought. Further, we discovered stable ''void'' spaces within the suspension, that contained low concentration of kaolin. Similar voids have been seen in both plasmas and suspensions of latex particles, and have been explained by the presence of many-body attractive forces. The discovery of such spontaneous voids occurring during kaolin sedimentation, may provide an explanation for the formation of water channels.

Author contributions

VVR did the experiments, all the simulations, data analysis, and writing original manuscript. WMH supervised the work and discussed the results. The paper was written and edited by both authors.

Data availability

The data in the figures, images and software used for simulations are available upon request.

Conflicts of interest

The authors declared no potential conflicts of interest with respect to the research, authorship, and/or publication of this article.

Acknowledgements

The authors thank Mr Jim Mullin for technical assistance. This work had no special funding from any foundation. However, this article is the development of an idea of WMH to apply MRI to studying channelling in gravity sedimentation, and it was performed due to research interests of VVR and WMH to this problem. It is not associated with a conference.

References

1 R. G. Holdich and G. Butt, Compression and channelling in gravity sedimenting systems, *Miner. Eng.*, 1996, **9**(1), 115–131.
2 A. De, *Sedimentation process and design of settling systems*., Springer, 2017.
3 Q. Chang, Sedimentation, *Colloid and interface chemistry for water quality control*, Academic press, 2016, ISBN 978-012-809315-3, pp. 23–35.
4 C. C. Dell and M. B. Kaynar, Channelling in flocculated suspensions, *Filtr. Sep.*, 1968, **5**, 323–327.
5 B. Fitch, A two-dimensional model for the free-settling regime in continuous thickening, *AIChE J.*, 1990, **36**(10), 1545–1554.
6 M. K. Cheung, R. L. Powell and M. J. McCarthy, Sedimentation of noncolloidal bidisperse suspensions, *AIChE J.*, 1996, **42**(1), 271–276.
7 P. Krishnamoorthy, Sedimentation model and analysis for differential settling of two - particle – size suspensions in the Stokes region, *Int. J. Sediment Res.*, 2010, **25**(2), 119–133.
8 I. R. McDermott, A. D. King, C. M. T. Woodworth–Lynas and P. LeFeuvre, In. Dewatering structures in high water content materials, *Geotechnics of High Water Content Materials, ASTM STP 13 74*, ed. T. B. Edil and P. J. Fox, American Society for Testing and Materials, West Conshohocken, PA, 2000, pp. 64–73.
9 Coulson and Richardson's Chemical Engineering, Sixth Edition, Vol. 2a: Particulate Systems and Particle Technology, *Sedimentation*, ed. R. Chabbra and M. G. Basavaraj, 2019, Ch. 8, pp. 387–447.
10 S. Nam, M. Gutierrez and P. Diplas, Channelling during settling and self-weighted consolidation of cohesive sediments, *Can. Geotech. J.*, 2008, **45**(6), 867–876.
11 P. A. Vesilind and G. N. Jones, Channelling in batch thickening, *Water Sci. Technol.*, 1993, **28**(1), 59–65.
12 P. A. Vesilind and G. N. Jones, A reexamination of the batch thickening curve, *Res. J. Water Pollut. Control Fed.*, 1990, **62**(7), 887–893.
13 B. Fitch, Sedimentation process fundamentals, *Trans. Am. Inst. Min. Eng.*, 1962, **223**, 129–137.
14 B. Fitch, Sedimentation of flocculent suspensions: State of the art, *AIChE J.*, 1979, **25**(6), 913–930.
15 G. J. Kynch, A theory of sedimentation, *Trans. Faraday Soc.*, 1952, **48**, 166–177.
16 G. K. Batchelor, Sedimentation in a dilute dispersion of spheres, *J. Fluid Mech.*, 1972, **52**(2), 245–268.
17 S. Vesaratchanon, A. D. Nikolov and D. T. Wasan, Collective particle interactions in the sedimentation of charged colloid suspensions, *Ind. Eng. Chem. Res.*, 2009, **48**(1), 80–84.
18 J. Gregory, The role of colloid interactions in solid-liquid separation, *Water Sci. Technol.*, 1993, **27**(10), 1–17.
19 S. Vesaratchanon, A. D. Nikolov and D. T. Wasan, Sedimentation in nano-colloidal dispersions: Effect of collective interactions and particle charge, *Adv. Colloid Interface Sci.*, 2007, **134–135**, 268–278.
20 J.-P. Hansen and H. Lowen, Effective interactions between electric double layers, *Annu. Rev. Phys. Chem.*, 2000, **51**(1), 209–242.
21 X. Chu and D. T. Wasan, Attractive interaction between similarly charged colloidal particles, *J. Colloid Interface Sci.*, 1996, **184**(1), 268–278.
22 J. Feng and E. Rukenstein, Attractive interactions in dispersions of identical charged colloidal particles: a Monte Carlo simulation, *J. Colloid Interface Sci.*, 2004, **272**(2), 430–437.
23 S. Dosho, N. Ise, K. Ito, S. Iwai and H. Kitano, *et al.*, Recent study of polymer latex dispersions, *Langmuir*, 1993, **9**(2), 394–411.
24 K. Ito, H. Yoshida and N. Ise, Void structure in colloidal dispersions, *Science*, 1994, **263**(5143), 66–68.
25 P. B. Warren, A theory of void formation in charge–stabilized colloidal suspensions at low ionic strength, *J. Chem. Phys.*, 2000, **112**(10), 4683–4698, DOI: **10.1063/1.481024**.
26 G. Praburam and J. Goree, Experimental observation of very low–frequency macroscopic modes in a dusty plasma, *Phys. Plasmas*, 1996, **3**(4), 1212–1219.

27 D. C. Dixon, In, *Progress in Filtration and Separation*, ed. R. J. Wakeman, Elsevier, Amsterdam, 1979, vol. 1.
28 B.-M. Wilen, *Effect of different parameters on settling properties of activated sludges*, WA-teknik, Chalmer, Rapport, 1995, vol. 4, pp. 1–53.
29 J. B. Madeline, M. Meireles, R. Botet and B. Cabane, The role of interparticle forces in colloidal aggregates: local investigations and modelling of restructuring during filtration, *Water Sci. Technol.*, 2006, **53**(7), 25–32.
30 M. Zurita-Gotor, J. Bławzdziewicz and E. Wajnryb, Layering instability in a confined suspension flow, *Phys. Rev. Lett.*, 2012, **108**, 068301.
31 A. K. Arora and B. V. R. Tata, Interactions, structural ordering and phase transitions in colloidal dispersions, *Adv. Colloid Interface Sci.*, 1998, **78**(1), 49–97.
32 X. Kang, Z. Xia, J. Wang. and W. Yang, A novel approach to model the batch sedimentation, and estimate the setting velocity, solid volume fraction and floc size of kaolinite in concentrated solutions, *Colloids Surf., A*, 2019, **A579**, 123647.
33 X.-Y. Ma, X. Kang, C.-X. Su, Y. Q. Chen and H.-M. Sun, Effects of water chemistry on microfabric and micromechanical properties evolution of coastal sediment: A centrifugal model study, *Sci. Total Environ.*, 2023, **866**, 161343.
34 T.-Q. Li, L. Ödberg, R. L. Powell and M. J. McCarthy, Quantitative measurements of flow acceleration by means of nuclear magnetic resonance imaging, *J. Magn. Reson., Series B*, 1995, **109**, 213–217.
35 S. D. Beyea, S. A. Altobelli and L. A. Mondy, Chemically selective NMR imaging of a 3- component (solid–solid–liquid) sedimenting system, *J. Magn. Reson.*, 2003, **161**(2), 198–203.
36 M. A. Turney, M. K. Cheung, M. J. McCarthy and R. L. Powell, Magnetic resonance imaging study of sedimenting suspensions of non-colloidal spheres, *Phys. Fluids*, 1995, **7**, 904–911.
37 M. A. Turney, M. K. Cheung, R. L. Powell and M. J. McCarthy, Hindering settling of rod like particles measured with magnetic resonance imaging, *AIChE J.*, 1995, **41**(2), 251–257.
38 S. Bobroff and R. J. Phillips, Nuclear magnetic resonance imaging investigation of sedimentation of concentrated suspensions in non-Newtonian fluids, *J. Rheol.*, 1998, **42**(6), 1419–1433, DOI: **10.1122/1.550895**.

